Validation of GlobSnow-2 snow water equivalent over Eastern Canada

Fanny Larue[1,2,3], Alain Royer[1,2], Danielle De Sève[3], Alexandre Langlois[1,2], Alexandre Roy[1,2] and Ludovic Brucker[4,5]

[1] Centre d'Applications et de Recherches en Télédétection, Université de Sherbrooke, Sherbrooke, Québec, Canada
[2] Centre for Northern Studies, Québec, Canada
[3] IREQ Hydro-Québec, Varenne, Québec, Canada
[4] NASA GSFC, Cryospheric Sciences Laboratory, Greenbelt, MD 20771, USA
[5] Universities Space Research Association, Goddard Earth Sciences Technology and Research Studies and Investigations, Columbia, MD 21044, USA

***** Correspondance: Fanny Larue, CARTEL, Département de Géomatique Appliquée, Université de Sherbrooke, 2500 Blvd. de l'Université, Sherbrooke, QC J1K 2R1, Canada.
E-mail address: fanny.larue@usherbrooke.ca

Abstract: In Québec, Eastern Canada, snowmelt runoff contributes more than 30% of the annual energy reserve for hydroelectricity production, and uncertainties in annual maximum snow water equivalent (SWE) over the region are one of the main constraints for improved hydrological forecasting. Current satellite-based methods for mapping SWE over Québec's main hydropower basins do not meet Hydro-Québec operational requirements for SWE accuracies with less than 15% error. This paper assesses the accuracy of the GlobSnow-2 (GS-2) SWE product, which combines microwave satellite data and *in situ* measurements, for hydrological applications in Québec. GS-2 SWE values for a 30-year period (1980 to 2009) were compared with space- and time-matched values from a comprehensive dataset of *in situ* SWE measurements (a total of 38 990 observations in Eastern Canada). The root mean square error (RMSE) of the GS-2 SWE product is 94.1 ± 20.3 mm, corresponding to an overall relative percentage error (RPE) of 35.9%. The main sources of uncertainty are wet and deep snow conditions (when SWE is higher than 150 mm), and forest cover type. However, compared to a typical stand-alone brightness temperature channel

difference algorithm, the assimilation of surface information in the GS-2 algorithm clearly improves SWE accuracy by reducing the RPE by about 30%. Comparison of trends in annual mean and maximum SWE between surface observations and GS-2 over 1980-2009 showed agreement for increasing trends over southern Québec, but less agreement on the sign and magnitude of trends over northern Québec. Extended at a continental scale, the GS-2 SWE trends highlight a strong regional variability.

Keywords: GlobSnow-2, passive microwave, *in situ* SWE measurements, Eastern Canada, land cover, water resources.

1. Introduction

Temperatures in Eastern Canada are expected to increase 2 to 4 degrees by 2050, which would result in a shorter snow period (SWIPA, 2011; Ouranos, 2015). Zhang et al. (2011) showed that while maximum snow depths in southern Canada can be expected to decrease as less cold-season precipitation falls in the form of snow, snowfall at high northern latitudes may increase by more than 10% in response to global warming (Räisänen, 2007; Brown and Mote, 2009; Brown, 2010). Seasonal snow cover has a strong impact on climatological and hydrological processes (Schultz and Barrett 1989; Albert et al., 1993). In the coming years, a good understanding of these trends will be needed to both improve long-term flow rate monitoring, and to address the significant economic impacts.

In Québec, Eastern Canada, one of the key variables in streamflow forecasting is the snow water equivalent (SWE), which describes the amount of water stored in the snowpack. For example, 1 mm of SWE in the headwaters of the Caniapiscau-La Grande hydro corridor (Québec) could represent $1M in hydroelectric power production

(Brown and Tabsoba, 2007). Optimal management of the snowmelt contribution to hydroelectric production requires accurate estimates of peak snow accumulation prior to spring melt (Turcotte et al. 2010). This is one of the main challenges for hydrological forecasting particularly over large remote watersheds. Current operational runoff forecast systems typically rely on surface snow surveys to determine pre-melt SWE, which can be supplemented with geostatistical interpolation procedures to provide a more detailed estimate of the spatial pattern (e.g. Tapsoba et al 2005).

However, manual snow surveys are time-consuming and expensive which make SWE estimation from satellite passive microwave (PMW) sensors an attractive option. PMW sensors also offer advantages of all weather and all year coverage at good temporal (daily) and moderate spatial (~25 km) resolution. The basic physics behind PMW SWE retrievals is that the natural emission measured by satellite-borne microwave radiometers, expressed as brightness temperature (T_B), is characterized by a high sensitivity to the volume of snow (Chang et al., 1987; Matzler, 1994; Tedesco et al., 2004). By performing multi-frequency combinations of measured T_B (typically at 19 and 37 GHz), the SWE can be estimated (Hallikainen and Jolma, 1992; Pullianen and Hallikainen, 2001; Parde et al., 2007; De Sève et al., 2007). However, this frequency range is resolved over relatively coarse spatial resolutions (~20 km). In Québec, factors such as the forest canopy, snow grain size (depth hoar), ice crust and lakes can have a strong impact on emission measured by satellite sensors and can cause high uncertainties in SWE estimates (up to 50% in boreal areas, Chang et al., 1996; Roy et al., 2004; Roy et al., 2010; 2012; 2015; Vachon et al., 2012). Several methods have been developed to constrain PMW SWE estimates by assimilating the T_B information into a snow model (Durand et al., 2009; DeChant and Moradkhani, 2011; Touré et al., 2011; Vachon et al., 2015).

In order to directly assimilate satellite-measured snow emission, Pulliainen (2006) proposed a technique that simulates PMW data by using ground-based snow depth measurements and a radiative transfer model. This assimilation protocol was integrated

84 into the European Space Agency's (ESA) GlobSnow project to estimate daily SWE time
85 series from 1979 to 2014 over the Northern Hemisphere (Takala et al. 2011, Luojus et al.,
86 2010). This historical dataset is freely available through the GlobSnow website
87 (www.globsnow.info, the database is regularly updated), and its gridded SWE data is
88 potentially of great interest to hydrological forecasters in Québec. In particular, Hydro-
89 Québec (HQ) decision makers have a need to better characterize the variability of snow
90 cover over watersheds to improve the performance of hydrological models. However,
91 while the GlobSnow-2 (GS-2) SWE product has been validated in Canada and globally
92 in previous studies (e.g. Hancock et al., 2013; Mudryk et al., 2015); its performance over
93 Eastern Canada has never been studied in detail.
94 The main purpose of this paper is to analyze GS-2 SWE values over an eco-climatic
95 and latitudinal gradient in Eastern Canada over a 30-year period to determine whether
96 it is accurate enough for hydrological applications, i.e., if the relative error in SWE is
97 lower than 15% which is the accuracy level required by HQ observing systems. The
98 CoreH20 satellite mission also set a performance objective at 15% (Rott et al., 2010), and
99 the ESA GS-2 project aimed to provide SWE maps for the Northern Hemisphere with a
100 root mean square error (RMSE) lower than 40 mm, i.e., an accuracy of 15% (Luojus et
101 al., 2014). As part of the evaluation, we also investigate the interannual variability and
102 trends in GS-2 SWE to determine its utility for hydroclimate monitoring. A unique
103 aspect to the evaluation is the use of a large database of 34 513 *in situ* SWE observations
104 covering the period of 1980 to 2009. These data were obtained from regular snow
105 surveys and field campaigns and are independent of the surface snow depth
106 observations assimilated into GS-2.
107 The four main goals of the paper are:
108 1. To determine if GS-2 performance meets HQ accuracy requirements, and to
109 analyse the global annual performance variability.

2. To evaluate the performance of GS-2 as a function of the various land cover types found over Eastern Canada (i.e. tundra, coniferous forest, mixed forest, deciduous forest). Biases due to wet and deep snow conditions are analysed and removed in order to only characterize the impacts of the land cover on the snow distribution over HQ's watersheds.

3. To determine the impact of assimilating surface observations into GS-2 compared to the AMSR-E typical stand-alone PMW SWE algorithm (Tedesco et al, 2004).

4. To compare trends in annual mean and maximum SWE over the 1980-2009 time period from surface observations and GS-2 to estimate the reliability of the GS-2 product for hydro-climate monitoring. To complete this analysis, the spatial variability of the trend of GS-2 maximum SWE anomalies is computed per pixel over North America.

2. Methods and data

2.1. Study area

The study area is located in Eastern Canada, between latitudes 45°N and 58°N (Fig. 1a). This region is characterized by significant snow cover and eco-climatic gradients: mean snow cover duration ranges on average from 120-240 days over the region (Brown, 2010), and vegetation ranges from open field, mixed forest, boreal forest and tundra moving north. Land cover was studied with the Land Cover Map of Canada (LCM, 2005), which has a spatial resolution of 1 km. Since the GS-2 SWE product was produced on the Northern Hemisphere Equal-Area Scalable Earth Grid (EASE-Grid), at a nominal resolution of 25x25-km (Armstrong et al., 1994), each EASE-Grid cell was classified according to its major fraction of land cover type in order to evaluate the contribution of the land cover (Fig. 1b). Table 1 presents the land cover classes used (seven in total) and the number of SWE measurements contained in the two databases

used (see Section 3). The Herbaceous class represents the open areas (crops) in southern Québec and dense forest areas were divided into three classes (coniferous, deciduous and mixed forest classes). The mixed forest class includes coniferous and deciduous forests, with both fractions greater than 30%. The Tundra class and the Northern open coniferous forest classES were grouped together to study the northern areas. Fig. 1b illustrates the aggregated land cover classification over Eastern Canada. SWE measurements located in an EASE-Grid cell with a predominantly urban fraction were removed to focus on natural surfaces.

The Global 30 Arc-Second Elevation (GTOPO30) dataset was used to compute the mean elevation of 25-km EASE-Grid cells to investigate the potential impact of topography when comparing *in situ* SWE observations to GS-2 grid averages.

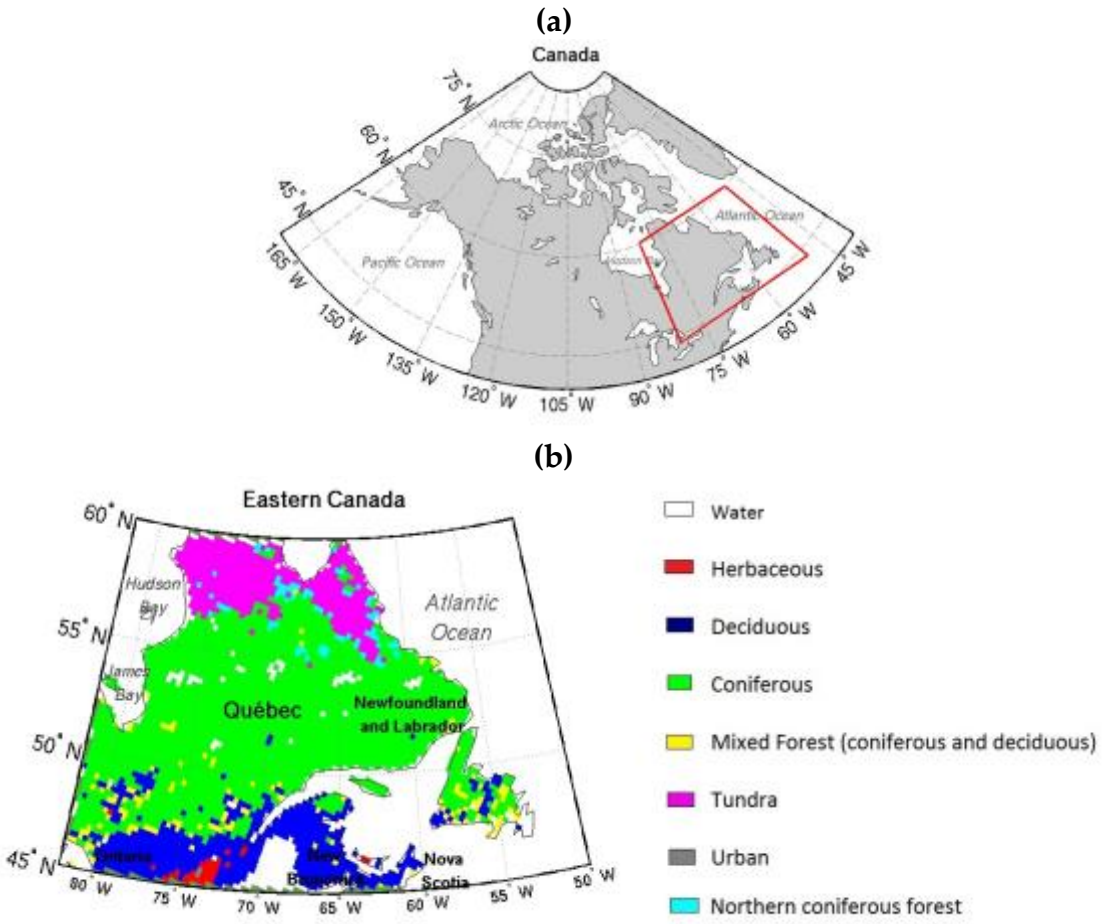

148 **Fig. 1.** (a) Location map of the study region (Eastern Canada); (b) Land Cover Map (LCM, 2005)
149 classification for Eastern Canada aggregated into eight classes and on the 25x25-km EASE-Grid
150 projection.

151

Table 1
Details of the land cover classification and of the number of SWE measurements from 1980 to 2009 (maj. = majority land cover type in the pixel) from the three main databases used in the present study: Database 1 is the complete *in situ* database, Database 2 has SWE values < 150mm and Database 3 is a subset of January-February SWE values < 150mm (see Sect. 2.5-B).

Areas	**Water**	**Open areas**	**Dense forest areas**			**Northern areas**		**Total**
Land cover	Water	Herbaceous	Deciduous	Coniferous	Mixed Forest	Tundra	Northern coniferous forest	-
Fractions: maj.	Water	Herbaceous	Deciduous	Coniferous	Conif. and Decid.	Tundra	Coniferous and Tundra	-
Number of SWE measurements in Database 1	526	2 420	17 702	11 963	1 748	7	147	34513
Number of SWE measurements in Database 2	338	2 215	11 640	3 575	951	4	104	18827
Number of SWE measurements in Database 3	167	1 336	5 771	1 652	463	4	43	9436

2.2. Reference measurements

This study grouped a unique historical database of ground-based SWE measurements (SWE_{gb}) from HQ (21 552 observations), the Meteorological Service of Canada (MSC) and the MDDEP (Ministère du Développement Durable, de l'Environnement et des Parcs du Québec, Québec) (17 389 observations). The dataset covers Eastern Canada, which includes the provinces of Québec, Nova Scotia, Newfoundland and Labrador, New Brunswick and Ontario (Figs. 1b and 2). About 1 163 stations were monitored every year from 1980 to 2009 (38 990 measurements). More specifically, the MSC conducted bi-monthly field surveys to estimate SWE through snow line from 1980 to 2003 (MSC, 2000; Brown 2007, 2010). In parallel, the MDDEP and HQ conducted field measurements at the end of each month from January to May plus mid-March, April and May to measure SWE, snow depth and density from 1980 to 2009 (Turcotte et al., 2007). The dataset used also observations acquired during

specific, short field campaigns by the University of Sherbrooke (49 SWE observations). In 2008, a 2000-km north-south snow measurement transect was carried out across Québec, from taiga to boreal forest, for the International Polar Year (Langlois et al., 2010). Two other field campaigns were also carried out in March 2003 and 2009 (Langlois et al., 2010, 2012).

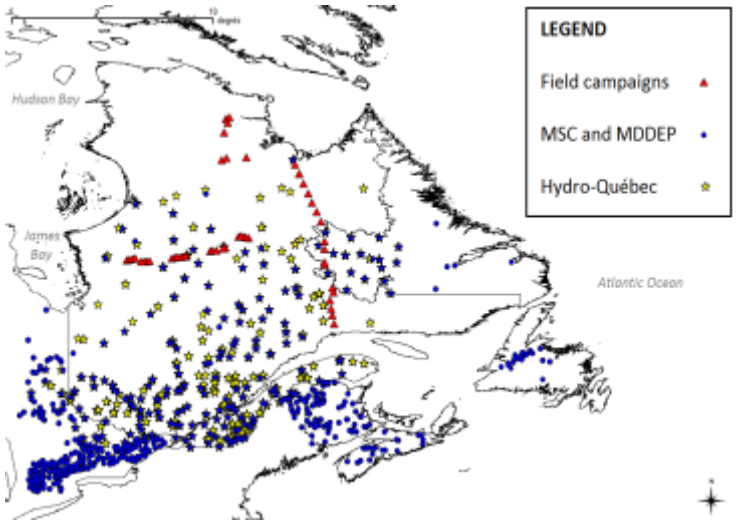

Fig. 2. Location of snow courses in the *in situ* SWE database (1980 to 2009). The blue stars are the superposition of the Hydro-Québec (yellow stars) and MSC/MDDEP snow surveys (blue points), sometimes taken at the same station over the 30-years period.

2.3. GlobSnow-2 SWE product

The GS-2 project provides SWE daily time series from 1979 to present, projected into the EASE-Grid by combining surface observations of snow depth (SD) in the PMW SWE retrieval (Takala et al. 2011). Takala (2011) describes the GS-2 SWE product in details, therefore only a brief description of the methodology is given here. The single layer HUT snow emission model is used to simulate T_B at each surface observation where SWE values are estimated from the observed SD, by assuming a constant snow density, and the HUT simulated T_B are assimilated with satellite observed T_B values by optimizing the effective snow grains sizes. Maps of the observed SD and the effective

snow grains sizes, produced by ordinary kriging interpolation to the 25-km EASE-Grid projection, are used to initialize the HUT model for each EASE-Grid cell and to generate gridded T_B simulations. The simulations are then assimilated with space-borne radiometer measurements by using adaptive weights on the observations according to their spatial and temporal variances (Pulliainen, 2006), and a map of SWE is obtained. A dry snow mask for each snow cover season is applied to the satellite radiometer data using the dry snow detection algorithm of Hall et al. (2002), as well as a mask to grid cells with more than 50% open water. The performance of this product is thus strongly linked to the spatial and temporal distributions of the SD observations used as input in the kriging tool that provides the gridded estimates of SD used in the retrieval. Fig. 3 shows the mean distance between SD observations used by GS-2 and 25-km EASE-Grid cells, from 1980 to 2012 (R. Brown, personal communication, 2016). Over Eastern Canada, we can see that there are major data gaps in the SD information over central and northern regions (distances higher than 200 km). Note that the data used for the evaluation of the present study are totally independent of those described in Fig. 3 and used by the GS-2 project.

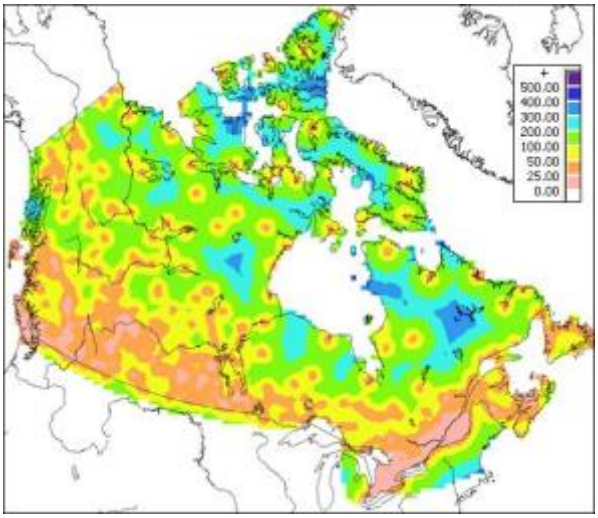

Fig. 3. Mean distance (in kilometers) between SD observations used by GS-2 project and EASE-Grid cells on which the GS-2 SWE are projected. The SD observations are those used by GS-2 from 1980 to 2012 (R. Brown, personal communication, 2016).

This product uses daily T_B (at 19 and 37 GHz in vertical polarization) from different satellite sensors: SMMR from 1979 to 1987, SSM/I from 1987 to 2009, and SSMIS from 2010 to the present. The inter-sensor bias in the satellite time series is not corrected (Takala et al., 2011) whereas previous studies have shown significant systematic biases in the T_B for the SMMR and SSM/I and SSM/IS sensors (see Bjørgo et al., 1997; Derksen et al., 2003; Royer and Poirier, 2010; André et al., 2015). The average SWE was estimated for each satellite sensor time period: the SWE_{GS} over southern Québec (south 50N) was equal to 102.1 mm and to 151.6 mm for northern Québec (above the 50th parallel north) for the 1980-1987 SMMR time period, and to 84.1 mm (144.2 mm) for the 1987-2009 SSM/I time period. The difference between the two mean SWE (over the SMMR period and over the SSM/I period) was around 10 mm with the GS-2 product and equal to 6 mm with the observations. The T_B changes between sensors, and while the pre-1987 SMMR data were expected to be less accurate, it appeared that the assimilation scheme may have compensated for them, leading to inter-sensor effects that were not statistically significant. Therefore, the inter-sensor bias was not taking into account for the analysis of the annual mean and maximum SWE trends.

229 *2.4. AMSR-E SWE product*

230 To evaluate the improvement associated with assimilating surface observations in
231 the SWE retrieval, the GS-2 product was compared with the stand-alone AMSR-E PMW
232 SWE product, distributed by NSIDC. For this inter-comparison, we used the AMSR-E
233 Level-3 daily SWE time series (SWE_{AMSRE}) on the Northern Hemisphere EASE-Grid
234 projection, with a spatial resolution of 25x25 km (Tedesco et al., 2004). This product is
235 available on the NSIDC website from June 2002 to October 2011, and is described in
236 detail by Kelly et al. (2003) and Kelly (2009). The SD is estimated by the attenuation
237 between T_B at 19 and 37 GHz and forest cover using the approach described in Chang
238 et al. (1987). Daily SWE_{AMSRE} values are then derived from microwave-retrieved SD and
239 ancillary snow density data.
240

241 *2.5. Stratification of the evaluation data with different criteria*

242 Before analyzing the forest cover impacts on the GS-2 product, the complete
243 database has been used to evaluate the GS-2 product and then stratified with different
244 criteria in order to study the importance of biases due to wet and deep snow conditions
245 in the Québec environment.

246 A) Matched measured and satellite-derived SWE values, 'Database 1': The GS-2
247 SWE product (SWE_{GS}) and the ground-based SWE measurements (SWE_{gb}) had to be
248 matched in space and time (daily), and coastal areas had to be avoided. When a SWE_{GS}
249 value was available, if there was more than one *in situ* measurement located within the
250 same EASE-Grid they were averaged to get only one ground-truth value per cell and
251 per date for comparison with the associated SWE_{GS} daily value. The initial complete
252 database included 38 990 SWE measurements. According to the 4 477 cases (11.5% of
253 the initial database) where we had more than one SWE observation for a same date and
254 a same grid cell and where we applied averaging, the mean standard deviation of SWE
255 measurements in a grid cell was 14.3 mm. A total of 34 513 matched SWE samples

remained after this procedure and this database, called 'Database 1', was used to quantify the global performances of the GS-2 SWE product.

B) Database without deep snow conditions, 'Database 2': It is well known that PMW SWE retrievals are underestimated under deep snow conditions (when SWE exceeds ~150 mm) because the snowpack transitions from a scattering medium to a source of emission due to the limited penetration depth at 37 GHz (Matzler et al., 1982; Mätzler, 1994; De Sève et al., 1997; De Sève et al., 2007; Luojus et al., 2010; Langlois et al., 2012). The exact value of this limit varies according to the snow grain size and stratification of the snow pack. Previous studies have shown that for the GS-2 SWE product, 150 mm was the critical threshold with Canadian reference datasets (Luojus et al., 2014). Fig. 4 illustrates that this detection limit was well defined at 150 mm for the present study area and beyond this value, SWE_{GS} values are significantly underestimated. The 'Database 2' regrouped all the data with SWE_{gb} below 150 mm in order to minimize the bias caused by the saturation of the penetration depth at 37 GHz in deep snow conditions (18 827 SWE data left from the 'Database 1').

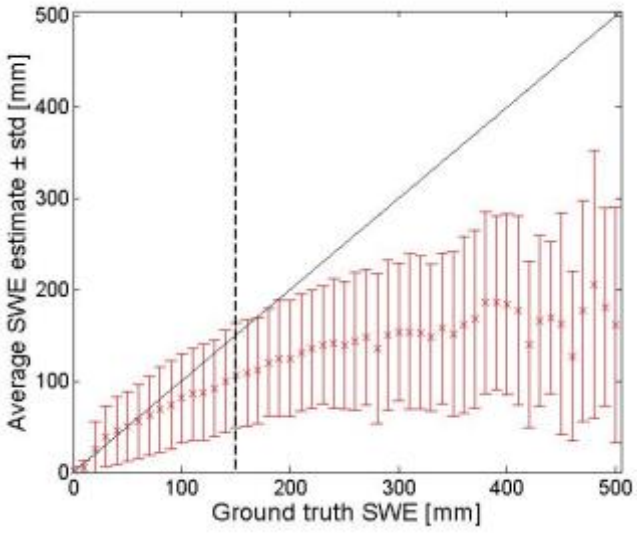

Fig. 4. GS-2 SWE product estimates as a function of *in situ* SWE measurements. The black vertical dotted line represents the saturation limit defined for this study. The Y=X line is also plotted in black.

C) Database without deep, shallow and wet snow conditions, 'Database 3': Eastern Canada is characterized by strong variability in the duration of seasonal snow cover according to latitude. Although the GS-2 SWE product is combined with a melt detection algorithm (Takala et al., 2009), uncertainties may persist in autumn (period from October to December) and later in spring (from Mars to June) because of difficulties in using radiometer data when a thin snow layer or wet snow exists (Klehmet et al., 2013). The performance of GS-2 in different snow climate regimes was carried out using the Sturm et al. (1995) seasonal snow classification. Fig. 5 shows the Sturm classification results with the Database 2 (SWE_{gb} < 150 mm) and Fig. 6 illustrates that the monthly bias is minimized for each snow category for the months of January and February. The evaluation database was then further stratified to include observations from January-February only to remove possible contamination from shallow or wet snow. This database, called 'Database 3' (9 436 SWE samples left from the Database 2), was used for the final analysis of the forest cover impacts.

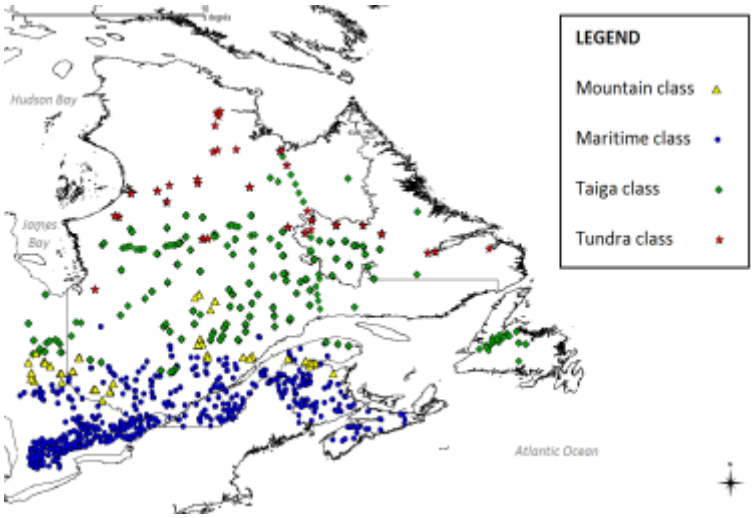

Fig. 5. Corresponding seasonal snow classification, based on Sturm et al. (1995), of the ground-based SWE measurements with the database without SWE_{gb}>150 mm.

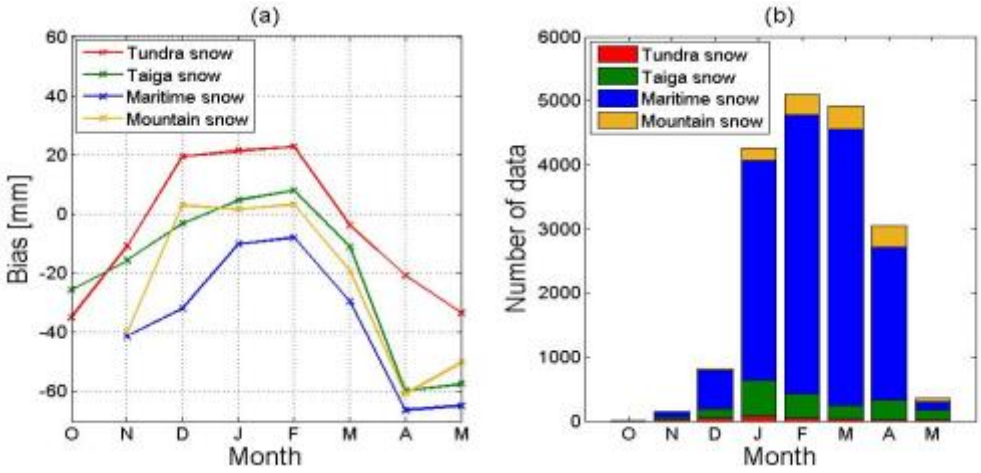

Fig. 6. Analysis for the dataset with SWE_{gb}<150mm and over the October to May period (1980-2009): (a) Monthly biases (SWE_{GS} - SWE_{gb}) according to the Sturm et al. (1995) seasonal snow classification; (b) Number of data points (SWE_{gb}) for each month by snow category: tundra (red), taiga (green), maritime snow (blue) and mountain snow (yellow).

Several metrics were used to evaluate the GS-2 algorithm. Differences between estimated and measured SWE (n cases) were analyzed using root-mean-squared-error (RMSE), unbiased RMSE (URMSE), standard deviation (STD), bias and the mean relative percentage of error (RPE) as validation metrics (Table 2).

Table 2

Validation metrics with j=year and i=1… n (number of SWE measurements per year).

Ground-based measurements and annual standard deviation		$SWE_{gb,\,j,i} = y_{j,i}$	$STD_{gb,j} = \sqrt{\frac{1}{n}\sum_{i=1}^{n}(y_{j,i} - \bar{y_j})^2}$	
GlobSnow-2 SWE product and annual standard deviation		$SWE_{GS,\,j,i} = x_{j,i}$	$STD_{GS,j} = \sqrt{\frac{1}{n}\sum_{i=1}^{n}(x_{j,i} - \bar{x_j})^2}$	
Metrics	$BIAS_j = \frac{1}{n}\sum_{i=1}^{n}[x_{j,i} - y_{j,i}]$	$RMSE_j = \sqrt{\frac{1}{n}\sum_{i=1}^{n}[(x_{j,i} - y_{j,i})]^2}$	$unbiaised\ RMSE_j = \sqrt{\frac{1}{n}\sum_{i=1}^{n}[(x_{j,i} - \bar{x_j}) - (y_{j,i} - \bar{y_j})]^2}$	*Relative Percentage Error (RPE)* $= 100.\frac{\lvert BIAS \rvert}{SWE_{gb}}$

2.6. Analysis of the annual mean and maximum SWE anomaly trends

Many recent studies have investigated possible annual mean and maximum SWE trends to analyse the evolution of the seasonal snow cover and have shown that global and regional warming have led to changes in snow accumulation, including declines and earlier dates of maximum SWE in many regions of the northern hemisphere (Mote et al., 2005; Stewart et al., 2005; Vikhamar-Schuler et al., 2006; Brown and Mote, 2009; SeNorge et al., 2009; Urban et al., 2014). To evaluate if the long-term time series of the GS-2 SWE product can be used for a long-term flow rate monitoring, tendencies obtained with the observed ground-based SWE and the GS-2 SWE over the same period (from 1980 to 2009) were compared, both for northern (Coniferous and Tundra classes) and southern Québec (Deciduous and Herbaceous classes). To avoid biases possibly caused by variability in the annual number of SWE measurements, and to improve the homogeneity of the dataset, only the HQ database was used in this section since it is the only one which extends from 1980 to 2009 over a December-March period ('Database 4', total of 13 999 SWE_{gb} from the Database 1). In addition, to compare trends without statistical noise due to local climatic differences, the anomalies are estimated by subtracting the annual mean variable by its overall average (over the 30-year time

period). Linear regression was used to analyze SWE trends over the 1980-2009 period with statistical significance assessed via a t-test at the 0.05 level.

The annual maximum SWE anomalies (noted SWE_{max}) are also of great interest to study the frequency of extremes and for hydrological purposes since they determine the water that will be released during spring runoff (Seidel and Martinec, 2004; Vachon et al., 2010). To study the SWE_{max} anomaly trends (departures from the 1980-2009 average) without being biased by abnormal extreme values, the annual SWE_{max} values were calculated as anomalies from the average of the five highest annual SWE estimated from December to March (with the Database 4).

Climate models suggest an increase of the maximum snow accumulation over southern Canada and a decrease over the tundra area in response to global warming (Brown and Mote, 2009; Zhang et al., 2011). In order to assess the spatial variability of GS-2 trends, the linear trend of the annual $SWE_{max,GB}$ anomalies (for the DJFM period, departures from the 1980-2009 average) has been computed per pixel at a continental scale (i.e. North America).

3. Results

3.1. GlobSnow-2 Data analysis

A) With the complete database: The results of the evaluation for the entire set of observations are provided in Table 3. With the Database 1, the unbiased RMSE and the bias are respectively equal to 76.5 mm and -54.8 mm (PE of 35.9%) which greatly exceeds HQ accuracy requirement of 15%. Nevertheless, as discussed in Sections 3.5 and 3.6, this product can provide useful spatial and temporal information to improve our knowledge on the seasonal snow cover trends, and therefore on the long-term flow rate monitoring to improve the performance of hydrological models (Hancock et al. 2013; Berezowski et al. 2015, Sospedra-Alfonso et al. 2016).

Table 3
Statistical results for the entire dataset (Database 1), for cases without high SWE_{gb} (SWE_{gb}<150mm, Database 2), and for cases with deep SWE_{gb} only (SWE_{gb}>150mm). The units for all statistics are mm.

	Number of data points	Mean SWE_{GS}	Mean SWE_{gb}	STD SWE_{GS}	STD SWE_{gb}	Unbiased RMSE (mm)	Bias (mm)	RMSE (mm)
Database 1: Entire dataset	34 513	97.8	152.6	66.8	83.4	76.5	-54.8	94.1
Database 2: With SWE_{gb}<150mm	18 827	71.1	91.3	50.2	34.7	49.0	-20.2	53.0
With SWE_{gb}>150mm only	15 686	129.6	225.2	69.9	63.0	82.8	-95.6	126.5

B) Effects of deep snow conditions: Table 3 shows the statistical results for GS-2 SWE product with SWE observations above and below the 150 mm upper detection limit for GS-2. With the Database 2, the overall unbiased RMSE (bias) is equal to 49 mm (-20.2 mm, RPE = 22%), whereas it reaches 82.8 mm (-95.6 mm) with SWE_{gb}>150mm. The errors measured under deep snow conditions are also strongly linked to the fixed snow density whereas the snowpack is often denser (Takala et al., 2011). In Eastern Canada, SWE measurements below 150 mm accounted for 55% of the dataset and this saturation can be highly significant, especially at the end of winter.

C) Effects of shallow and wet snow conditions**:** Table 4 presents the seasonal statistics for the three main time periods of interest from the Database 2 (fall, winter and spring). Even if the unbiased RMSE remains relatively similar (between 43 and 47 mm) regardless the period, the bias is considerably reduced with the Database 3, i-e for the January-February period (-2.7 mm compared to -20.2 mm for the whole period with the Database 2).

371 **Table 4**
372 Seasonal statistics for the three main time periods of interest: fall (October-November-December), winter
373 (January-February), spring (Mars-April-May-June). The entire winter period (D-J-F-M: from December
374 to March) is also studied. The database used is the one without high SWE_{gb} (Database 2: SWE_{gb}<150 mm).

Time Period	Number of data points	Mean SWE_{GS}	Mean SWE_{gb}	STD SWE_{GS}	STD SWE_{gb}	Unbiased RMSE (mm)	Biases (mm)	RMSE (mm)
Database 2: Annual with SWE_{gb} < 150 mm	18 827	71.1	91.3	50.2	34.7	49.0	-20.2	53.0
Fall (O-N-D)	552	44.7	63.4	50.6	30.4	43.4	-18.7	47.3
Spring (M-A-M-J)	8 839	58.1	97.2	48.5	34.3	47.1	-39.1	61.2
Database 3: Winter (J-F)	9 436	84.7	87.4	48.0	34.0	44.3	-2.7	44.4
Winter (D-J-F-M)	15 317	80.7	91.2	48.5	34.7	45.9	-10.6	47.1

375

376 *3.2. Global performance variability*

377 To analyze the accuracy of the GS-2 SWE product without the limit cases potentially
378 caused by shallow, deep and wet snow conditions, we assessed the time variability of
379 the GS-2 with the three databases described in section 3.5. Fig. 7 shows the global
380 statistics for each database. The overall URMSE and bias obtained with the Database 1
381 are 76.5 mm and -54.8 mm respectively, corresponding to a percentage of error of 36 %
382 (Table 3). With the Database 3, by taking SWE_{gb} < 150 mm over January-February only,
383 the inter-annual variability in the uncertainty (URMSE) is reduced by - 42% to 44.3 mm,
384 and the bias is reduced by -95% to -2.7 mm (RPE of 3.1%, Table 4). The observed
385 interannual variability corresponds to variations in meteorological conditions, mainly
386 fall and spring melt periods, as well as years with deeper snowpacks (Fig. 7c). Even if
387 the reference ground-based stations are relatively well distributed over the southern
388 part of the studied area (Fig. 2), the variations in Fig. 7 could also possibly be affected
389 by monthly and yearly variations in the number of stations in the different databases
390 (see Fig. 6). The database includes a peak of data collection between 1984 and 2002
391 (around 1500 SWE measurements per year), with a reduction in field measurements
392 before and after (< 1000 data/year) (e.g. Brown, 2010). A high bias appears for the 2004-
393 2009 period, for which we only have HQ data. However, the HQ dataset has the best

spatial distribution of the datasets used in this study (Fig. 2). Furthermore, this period corresponds to a high mean SWE measured value (Fig. 7c).

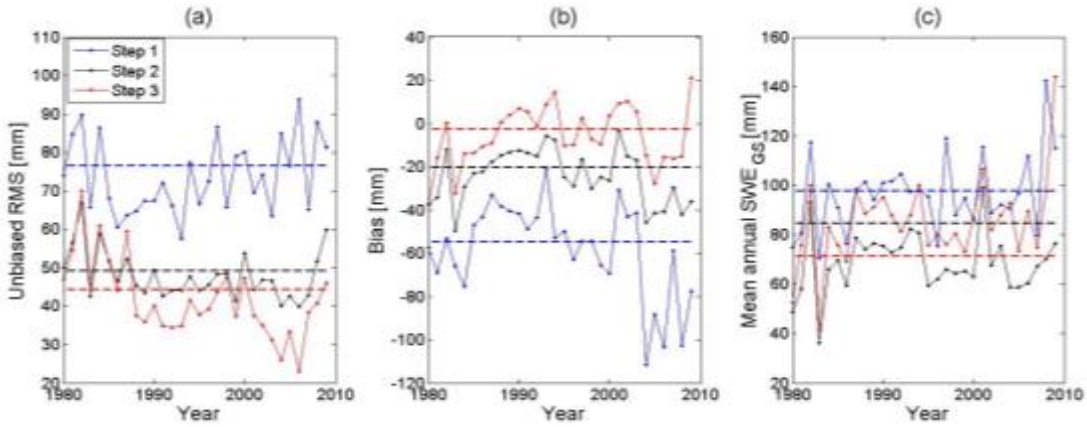

Fig. 7. Global performance statistics for each processing step: the entire dataset with matching data (black, Step 1), only with SWE_{gb}<150mm (blue, Step 2) and over the January-February time period (red, Step 3). The graphs present the inter-annual variability of the unbiased RMSE (a); the inter-annual variability of the bias (b) and the inter-annual variability of the average SWE_{GS} (c). The dotted lines are the average of the time series from 1980 to 2009.

Without the effects of deep and wet snow conditions, the SWE_{GS} reaches the targeted accuracy, with a relative percentage error below 15%. Nevertheless, it appears that even in the most favourable conditions, the RMSE rarely goes below the GS-2 targeted threshold of 40 mm. Comparing point-level measurements to the 25x25 km resolution GS-2 database involves uncertainty due to SWE spatial variations. However, the large number of comparisons performed (34 513 point-level SWE measurements matched with GS-2 pixels) and the random spatial localization of point-level measurements within pixels (for those particular pixels having several matched ground-based measurements) provides a useful assessment of GS-2 results. The estimated average standard deviation of SWE measurements (estimated in Section 2.5), when several data points fall within the same EASE-Grid cell, is relatively low (14.3 mm) compared to the RMSE. In addition, an analysis of SWE_{GS} sensitivity to the distance between the point-level SWE measurements and the center of the associated EASE-Grid cell (not shown) does not exhibit a particular trend.

418

419 *3.3. Effects of land cover*

420 Lakes are known to have a different snow cover with thinner and denser snow
421 (wind slab) than surrounding areas (Green et al., 2012; Sturm and Liston, 2003).
422 Moreover, lake ice under snow and its thickness can have a strong impact on the
423 microwave signal (Kang et al., 2010). Nevertheless, the GlobSnow-2 SWE product
424 includes a mask applied for grid cells with more than 50% fraction of open water and
425 an analysis of the effects of lake fraction and topography (not shown) found no evidence
426 that either of these played a significant role in the evaluation results (P-values < 0. 001).

427 The forest cover fraction can also have a strong impact on the seasonal snow
428 distribution in boreal areas (Foster et al., 2005; Derksen et al, 2005; Derksen et al., 2008).
429 Fig. 8 shows the unbiased RMSE (URMSE) according to the forest cover fraction (=
430 deciduous fraction + coniferous fraction) and estimated with the Database 3. The
431 URMSE is fitted with a simple quadratic function to show the general shape. There is a
432 significant upward trend of the URMSE according to the percentage of forest in an
433 EASE-Grid cell of 25x25 km of resolution. In forested areas, uncertainties are mostly
434 due to snow-vegetation interactions that strongly affect snow cover variability
435 (especially with different types of forests) and the vegetation contribution (emission
436 and transmission), which are difficult to model precisely in an inversion scheme (Roy
437 et al., 2012; Vachon et al., 2012). The SWE data included in grid cells with more than
438 90% forest cover represent 38% of the observations and have a URMSE higher than 50
439 mm.

440

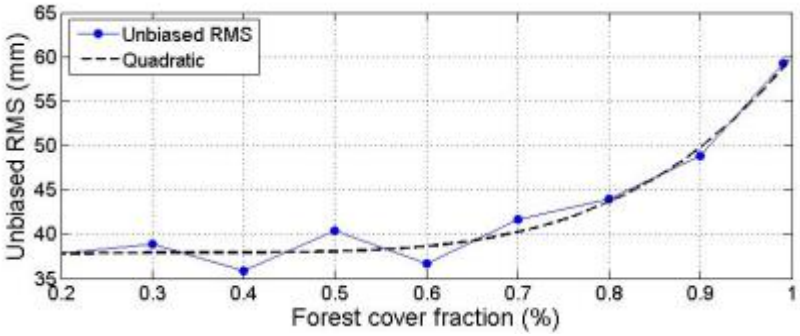

Fig. 8. Unbiased RMS according to the forest cover fraction (in %). The unbiased RMS is fitted with a simple quadratic function (black dotted line).

The SWE_{GS} values were compared to the ground-based measurements for each land cover category (Fig. 9). A summary of the SWE_{GS} sensitivities is provided in Table 5. By only keeping $SWE_{gb} < 150$ mm collected over the winter period (Database 3), the overall bias of boreal areas is reduced and is particularly low (-2.5 mm) compared to the complete database (-57.9 mm, RPE = 37%). The lowest unbiased RMSE concerns the tundra class (32.2 mm), but this is also the class with the strongest bias. Corrections have been applied in these northern areas with the GS-2 project by using comprehensive ground measurement campaigns in the Northern Territories, Canada (Takala et al., 2011). However, note that the statistics of this class are sensitive to the small amount of data to assess in comparison to other classes. The retrieval uncertainties are highest for the coniferous class, where the unbiased RMSE is 47.6 ± 15.1 mm. This class is characterized by deep boreal forest snow, with an average SWE_{gb} > 100 mm (Table 5, Fig. 9a), and snowpack microwave signals that are much more influenced by interactions with snow grains (the larger the grains, the earlier saturation occurs), which are not well resolved in 1 layer GS-2 processing. Moreover, the coniferous class corresponds to the central region of Québec, where the SD observations used by GS-2 are very limited (see Section 2.3, Fig. 3), which increases uncertainties of interpolated snow depth maps used in the assimilation process. In southern boreal forest areas (deciduous and mixed forest), an overall unbiased RMSE of 45.0 ± 10.5 mm

and an overall bias of -2.1 ± 15.1 mm (relative error of 2.3%) are found (Table 5). The distribution of SWE values in the deciduous class are uniformly distributed between 35 mm and 130 mm (Figs. 9b and 9c) and the high RMSE estimated for this class is mostly linked to the presence of dense vegetation and the different forest cover types. The deviation is lower for open areas (herbaceous class) in southern Québec, with a mean bias of -1.2 ± 14.4 mm and an unbiased RMSE of 36.3 ± 9.5 mm (Table 5). Note that this land cover is characterized by shallower snow cover (average SWE_{gb} < 100 mm), not affected by dense vegetation, and the high number of SD observations in this region helps to reduce uncertainties (Fig. 3).

The most important hydrological structures in Québec are located in boreal forest areas in the James Bay region. In this area, the GS-2 SWE product reasonably captures SWE values with an overall error (RPE) of 3% (Table 5 for boreal area), without wet snow conditions, and only for snowpack below 150 mm of SWE, which do not correspond to the conditions often observed at the end of winter. With the complete database, over the boreal forest areas, the mean percentage error increases to 36.6% (RMSE = 97.1 mm, and URMSE = 77.9 mm). Over the James Bay region, the SWE_{GS} is thus not accurate enough to be used in an operational hydrological context (error > 15%).

Moreover, GS-2 uses a constant value for snow density whereas the density is higher in late winter due to the snow metamorphism. The ESA GlobSnow-2 project has tried to use a dynamic density to describe the evolution of seasonal snow cover but the results did not show significant improvement and a constant density is still used. This generates a decrease in the SWE_{GS} accuracy, especially at the end of winter.

Even if the results of the present study reasonably capture the uncertainty trends estimated by the ESA study for the Canadian land cover region (*GlobSnow-2 Final Newsletter*, ESA; Derksen et al., 2008), we systematically found higher uncertainties and biases.

Table 5

Summary of performance statistics for each land cover category over Eastern Canada. Database 1 is the complete database. Database 3 is the database without SWE_{gb} > 150 mm and over a period from January to February. r is the correlation coefficient. The boreal forest class includes deciduous, coniferous and mixed forest classes.

	Area	Land cover	Number of data	Mean SWE_{GS} (mm)	Mean SWE_{gb} (mm)	STD SWE_{GS} (mm)	STD SWE_{gb} (mm)	Unbiased RMSE (mm)	Bias (mm)	RMSE (mm)	r
Database 1	**Boreal Forests**		31 413	100.4	158.3	67.9	83.8	77.9	-57.9	97.1	0.49
Database 3	**Total**		9 436	84.7	87.4	48.0	34.0	44.3	-2.7	44.4	0.46
	Boreal Forests		7 886	87.3	89.8	49.1	33.9	45.3	- 2.5	45.4	0.45
		Coniferous	1 652	113.8	108.5	50.7	27.8	47.6	5.3	47.9	0.39
		Deciduous	5 771	79.2	84.3	45.9	33.6	44.3	- 5.1	44.6	0.42
		Mixed Forest	463	93.6	92.6	47.7	32.0	45.7	1.0	45.8	0.38
	Open areas	**Herba-ceous**	1 336	71.5	72.7	35.9	31.1	36.3	- 1.2	36.4	0.41
	Subarctic snow	**Tundra**	47	109.7	85.3	38.4	32.2	32.5	24.4	40.7	0.58

498

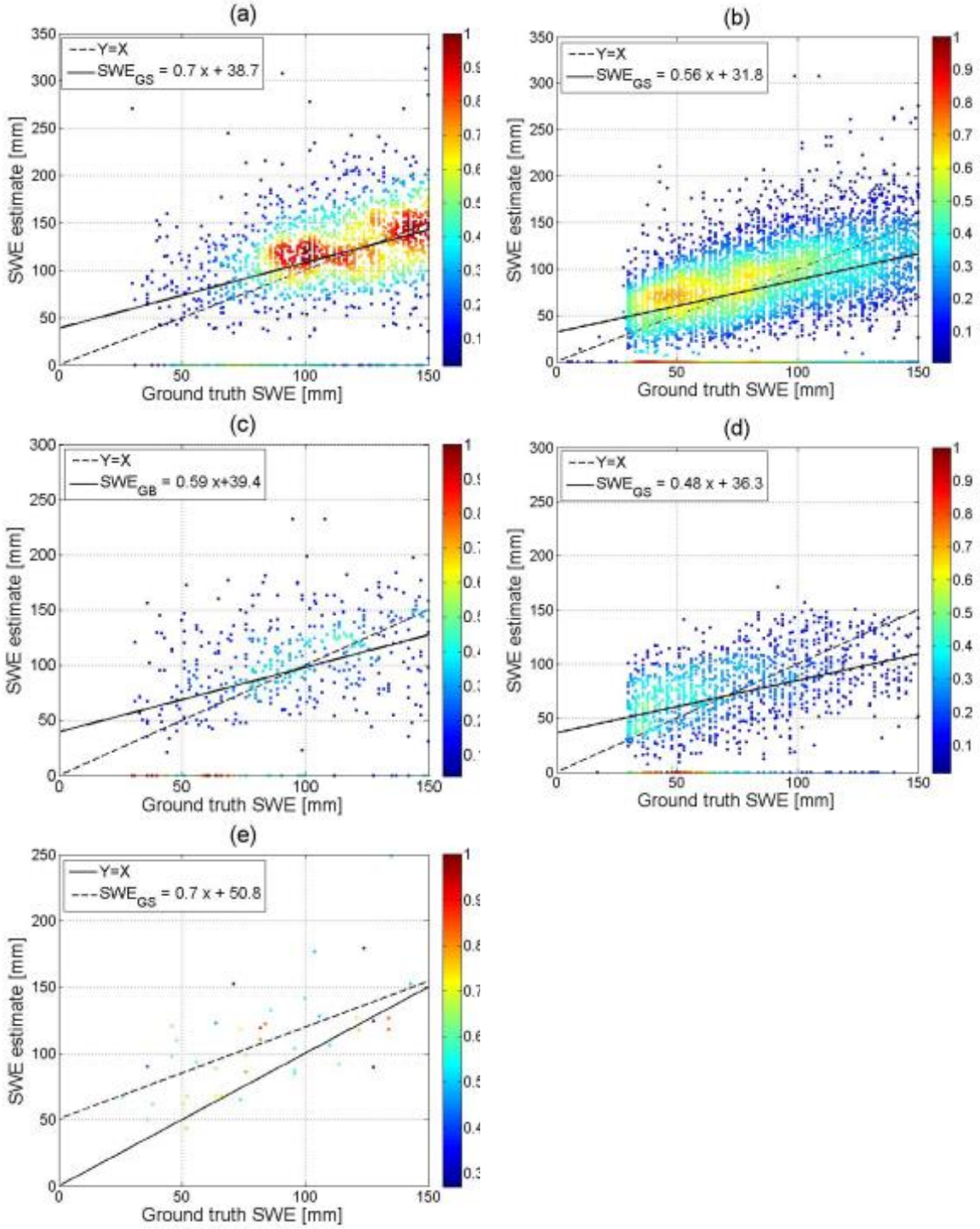

499 **Fig. 9.** Evaluation of the GS-2 database for Eastern Canada, SWE_{GS} are compared to ground-based
500 measurements (using Database 3) for each land cover class: (a) Coniferous; (b) Deciduous; (c) Mixed
501 forest; (d) Herbaceous; (e) Tundra. The color scale represents the data density of scattered points,
502 computed by using circles (radius of 20) centered at each data point.

503

504

3.4. Comparison with the AMSR-E SWE product

The AMSR-E SWE product (SWE_{AMSRE}) and GS-2 SWE_{GS} results were compared to *in situ* observations from 2002 to 2009, for January-February only (total of 2 128 SWE matched data points). Fig. 10 shows results for both products, while Table 6 gives detailed statistics for each database. Over Eastern Canada, SWE_{AMSRE} is particularly underestimated and shows a large RMSE of 165.6 mm, with very weak SWE variability. This approach seems to be affected by several contributions within the same cell, since radiation is particularly affected by land cover as well as by snow grain morphology (grain size, grain morphology, refreezing crust) and snow condition (dry and wet snow), which are conditioned by climate conditions (Dong et al., 2005). Consequently, the accuracy of SWE_{AMSRE} is particularly low for deeper snowpacks, especially when SWE is higher than 60 mm (Fig. 10). The effects of vegetation and lakes also produce complex microwave signals, which have a negative impact on the SWE retrieval (Foster et al., 2005). Indeed, the variation of land cover percentage within grid cells, more specifically forest and water, greatly affects the radiometric value measured by satellites. Forest emissivity may be very high (close to 0.9), and it hides the signature of the underlying snow. In addition, when ice is forming over water surfaces, the upwelling radiation of lakes at high frequencies (85 and 37 GHz) comes mainly from the ice cover, which behaves as a microwave emitter. Thus, any increase in percentage of "thin snow covered lake ice" within a pixel could increase its radiometric value. At lower frequency, the contribution of water bodies acts as a specular reflector and the emissivity remains low (De Sève et al., 1999). The GlobSnow-2 algorithm, which combines information from both satellite observations and ground-based snow-depth measurements through an assimilation process, improves the estimates of SWE with an overall RMSE of 71.1 mm. The overall bias (-36.1 mm) is clearly lower than the one obtained with SWE_{AMSRE} (-90.2 mm) (Table 6). The SWE_{GS} is less sensitive to deep snow conditions, although for SWE values above 150 mm this sensitivity is high (see Section

532 3.1). These results, which show the improvement obtained by using the GlobSnow-2
533 assimilation algorithm over Eastern Canada (below 58°N), are in agreement with those
534 obtained by the ESA program for Finland between 2005 and 2008 (Luojus et al., 2014).
535

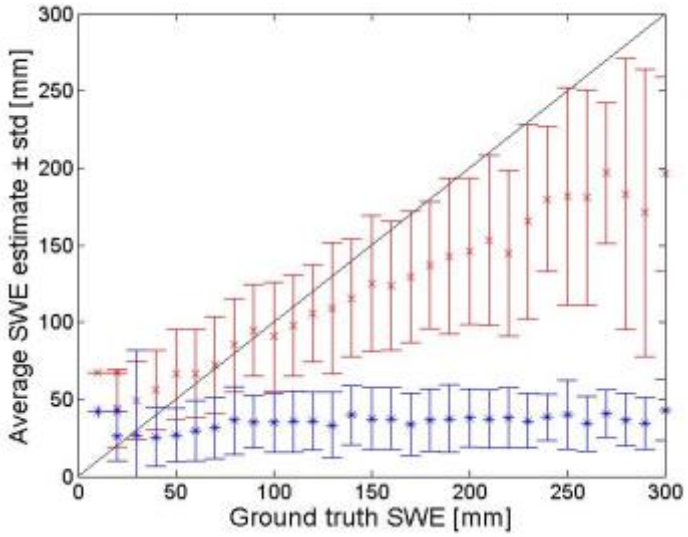

536

537 **Fig. 10**. The SWE_{AMSR-E} and GS-2 SWE results are compared to *in situ* observations from 2002 to 2009,
538 for January-February only.

539
540 **Table 6**
541 Summary of performance metrics for the AMSR-E product (SWE_{AMSRE}) and the GS-2 SWE product
542 (SWE_{GB}) from 2002 to 2009, for January-February only.

	SWE_{gb}	SWE_{AMSRE}	SWE_{GS}
Mean (mm)	154.3	64.2	118.2
STD (mm)	76.0	111.4	59.2
RMSE (mm)		165.6	71.1
Bias (mm)		- 90.2	- 36.1
PE (%)		58.1	23.4

543
544

545 *3.5. Evaluation of the annual mean and maximum SWE trends*

546 Figs. 11a and 11b show the inter-annual variabilities of the yearly mean SWE
547 anomaly, for northern and southern Québec respectively, and estimated with the
548 Database 4 (see Section 2.6). For the southern area, linear trends show an increase for
549 both the GS-2 product and observations (slope of 1.4 and 0.6 mm/year respectively). For
550 the northern region the observed trends are not significantly different from zero (slope
551 of 0.8 and 0.3 mm/yr respectively). The temporal trends of the annual mean SWE
552 anomaly are not statistically significant (p-value<0.01) and the inter-annual variations
553 between annual mean SWE_{GS} and SWE_{gb} appear relatively consistent.

554 The measured SWE_{max} values averaged over the Québec area occur generally in
555 February: maximum SWE are 266.9 ± 49.5 mm for February and 143 ± 148.6 mm for
556 March in the north, while the corresponding values for the south are respectively 187.5
557 ± 51.4 mm and 102 ± 113.5 mm; but note the strong variability (standard deviation) in
558 March. Fig. 11c (11d) shows the SWE_{max} anomaly trends estimated for the southern
559 (northern) regions described above. In the south, the $SWE_{max,GS}$ anomaly trend suggests
560 a significant increase in snow accumulation in agreement with observations (slope of
561 3.2 and 2.0 mm/yr respectively). In contrast, over the northern area, the $SWE_{max,GS}$
562 anomaly trend suggests a decrease (slope of -0.7 mm/yr), which is not consistent with
563 the measurements (slope of +1.5 mm/yr). Note that Figs. 11c and 11d show strong
564 variability of the inter-annual SWE_{max}, as discussed by Brown (2010). It has been shown
565 that, over the past six decades, Québec is particularly subject to regional variability of
566 the inter-annual $SWE_{max,}$ especially during the spring (Vincent et al., 2015), which
567 complicates the analysis over only two areas in Québec.

568

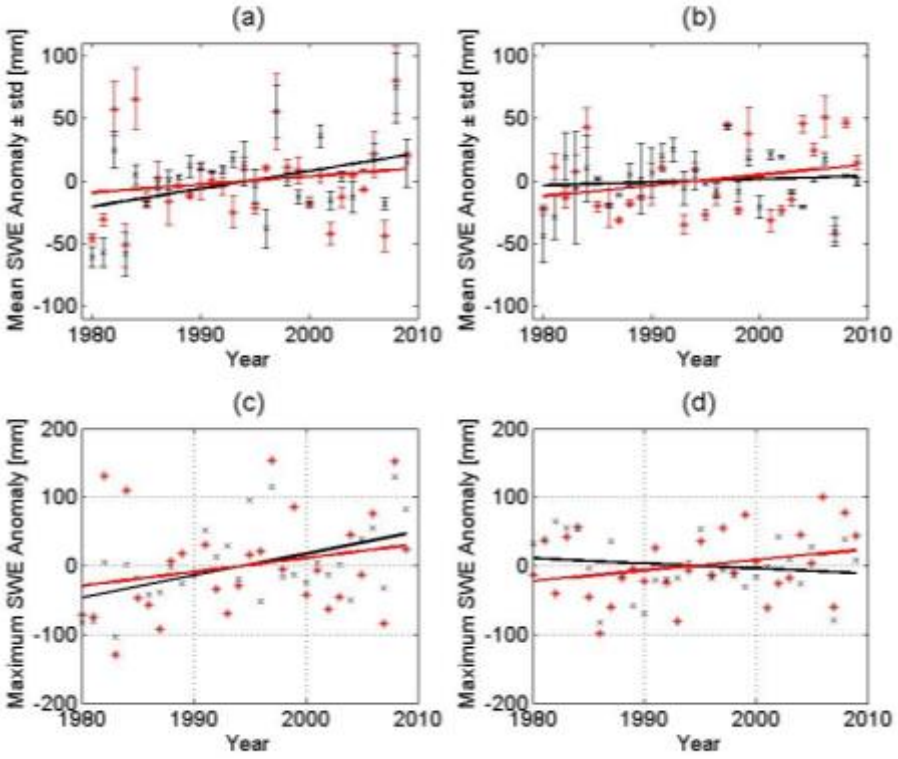

569

570 **Fig. 11.** (a) Annual mean SWE anomaly time series, associated with the standard deviations for both
571 datasets (ground database in red and GS-2 database in black), and over the southern area, defined by the
572 herbaceous and deciduous areas**.** (b) Same as (a) for the northern area, defined by the coniferous and
573 tundra areas. (c) Same as (a) for the maximum SWE anomaly time series. (d) Same as (b) for the maximum
574 SWE anomaly time series. The lines represent the linear SWE regression in time. The complete Hydro-
575 Québec database from 1980 to 2009 was used, over a December to March period.

576

577 *3.6. Spatial variability of the trends of GS-2 maximum SWE anomalies over North America.*

578 Fig. 12 shows the anomaly trend in the annual $SWE_{max,GS}$ for the period 1980-2009
579 over North America. Results stress a significant positive trend across the maritime area
580 of Québec, where an important number of snow surveys used in previous sections are
581 located. This probably led to the positive trend of SWE_{max} anomalies previously shown
582 (Fig. 11c) for southern area of Québec (delimited by deciduous and herbaceous classes).
583 Overall, across Canada and Alaska, there is important regional variabilities with a
584 general North-South contrast of the $SWE_{max,GB}$ anomaly trends (decreasing trend in the
585 North and increasing trend toward the South), in agreement with the annual measured

maximum snow depth anomalies obtained by Zhang (2011) from 1950 to 2007, also documented in Vincent and Mekis (2006). However, over north-western Alaska area, the $SWE_{max,GS}$ trend significantly increases as predicted by model consensus over Arctic high latitudes (Brown and Mote, 2009).

The similarities between annual maximum GS-2 and *in situ* SWE trends shown in Section 3.5 (also observed for the bias trend, relatively constant, between both datasets over time) for the Québec area, validated to extend the analysis at the continental scale (i.e. North America), highlighting a strong regional variability. The annual maximum SWE anomaly trend in response to global warming is difficult to analyse, given its link with both variations on precipitations falling as snow and temperatures, and appear less spatially coherent. Moreover, the SWE_{max} variable is highly sensitive to metamorphism within the snowpack, impacting the snow density evolution which is sensitive to regional climate conditions. These processes, difficult to capture using satellite remote sensing, could lead to errors in the interpretation of climate change impacts on snow evolution.

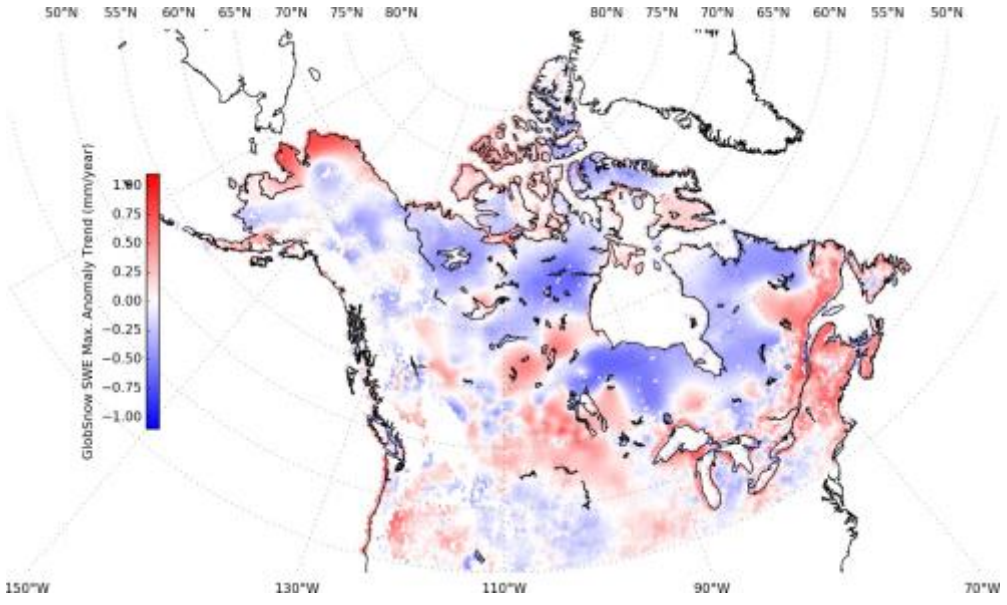

Fig. 12. Anomaly trend in the annual SWE_{max} for the 1980-2009 period using the GS-2 time series.

4. Summary and conclusions

This study evaluates the GS-2 SWE product over an eco-latitudinal gradient in Eastern Canada using an extensive ground-based dataset. The assimilation approach used to estimate GS-2 SWE values clearly improves the accuracy level by reducing the relative percentage of error by about 30%, compared with a typical stand-alone algorithm based on T_B channel difference (SWE_{AMSR-E}). Over the study area, which was mainly forested, the RMSE between GS-2 and ground-based SWE data is 94.1 ± 20.3 mm with the complete database (Database 1); which is significantly higher than the objective of 40 mm. Without wet snow and deep snow conditions (Database 3), the GS-2 SWE root mean square error was about 44.4 ± 10.4 mm, with a coefficient of correlation (R) of 0.46. Retrieval sensitivity to land cover and forest cover fraction has been studied: the highest SWE uncertainties were for dense boreal forest areas, showing that the effects of both dense vegetation and deep boreal forest snow on the microwave signal can have significant impacts on this product. There is an exponential trend of the unbiased RMS for SWE_{GS} according to the fraction of forest cover, but the impact on RMSE is relatively small for forest fraction below 70% in a 25km EASE-Grid cell. In addition, a comparison of biases with and without the 150-mm threshold on SWE_{gb} (-20.2 mm and -54.8 mm, respectively) shows that deep snow conditions are a major source of uncertainties in algorithms using T_B, due to the saturation of the penetration depth at 37 GHz.

The sparse distribution of SD observations used by GlobSnow-2 in northern areas of Eastern Canada prevents the capture of the spatial and temporal SWE variability required in an operational context for hydrological applications. Hydropower management requires SWE biases lower than ~20 mm for typical winter snowpack conditions over Eastern Canada (average SWEmax ~150 mm to meet accuracy requirements of 15%). In Eastern Canada, according to 34 513 matched SWE measurements, the overall percentage of error of the GS-2 SWE product is 35.9% and

632 the bias is -54.8 ± 21.9 mm. Over boreal forest areas, where the most important
633 hydrological complexes are located in Québec, the relative percentage error increases
634 to 36.6% (RMSE of 97.1 ± 20.3 mm and bias of -57.9 ± 22.2 mm). Nevertheless, the GS-2
635 product can provide useful information about the overall spatial and temporal snow
636 cover distribution to improve hydrological model simulations, especially at the
637 beginning and end of the snow season, before snowmelt (Hancock et al. 2013;
638 Berezowski et al., 2015; Sospedra-Alfonso et al., 2016). Indeed, assimilation allows to
639 correct model error or input uncertainties with a more relaxed accuracy requirement as
640 long as the uncertainty of the data is known (Quaife et al., 2008; Lewis et al., 2012). To
641 accurately map SWE, more complex approaches, which take into account a range of
642 parameters in the assimilation process, should be explored. Given the sensitivity of
643 SWE to precipitation and to metamorphism associated with the winter climate, the use
644 of a snow model coupled with a radiative transfer model to assimilate T_B by optimizing
645 the initialization of atmospheric variables appears to be a promising approach (Durand
646 et al., 2009; Brucker et al. 2010, Langlois et al., 2012). This technique could allow us to
647 estimate a SWE without the need for ground data and represents an interesting
648 alternative for remote areas.

649 The bias between the annual mean SWE anomaly trends between both observed
650 and GS-2 data for long-term observations (over 30 years) appear relatively constant.
651 The average SWE_{GS} time series can help us to better understand climate impacts, and
652 thus to adapt monitoring tools for hydrological operations, whereas the annual
653 maximum SWE_{GS} trend has to be used carefully given the high regional variability of
654 the inter-annual $SWE_{max.}$

655

656 **Acknowledgements.** The authors would like to thank Lucie Lozach (Centre d'Applications et
657 de Recherches en Télédétection, University of Sherbrooke) for assistance in database processing
658 and Chris Derksen (Environment Canada) for providing some SWE data. A special thanks to
659 all the data providers: National Institute for Scientific Research of Québec and Hydro-Québec, the

European Space Agency, the NSIDC, the Finnish Meteorological Institute, the MSC and the MDDEP. This project was supported by NSERC-Canada, MITACS, IREQ and FRQ-NT-Québec. The authors also thank both reviewers and the editor for their insightful comments, in particular Ross Brown (Environment Canada, Montréal).

References

Albert, M. R., J. P. Hardy, and P. Marsh (1993). *An introduction to snow hydrology and its integration with physical, chemical and biological systems.* Snow Hydrology: The Integration of Physical Chemical and Biological Systems, J. Hardy, M. R. Albert, and P. Marsh, Eds., John Wiley and Sons, 373 pp.

André C., C. Ottlé, A. Royer, and F. Maignan (2015). Land Surface Temperature Retrieval over circumpolar Arctic using SSM/I-SSMIS and MODIS Data, *Rem. Sens. of Enviro.*,162, 1-10.

Andreadis, K. M. and D. P. Lettenmaier (2006). Assimilating remotely sensed snow observations into a macroscale hydrology model. *Adv. Water Resou.* 29, 872–886.

Armstrong, R. L. and M. J. Brodzik (1999). A twenty year record of global snow cover fluctuations derived from passive microwave remote sensing data. In: *Fifth Conf. on Polar Meteorology & Oceanography,* 113-117. Am. Met. Soc, Dallas, Texas, USA.

Armstrong, R. L., K. W. Knowles, M. J. Brodzik, and M.A. Hardman (1994). updated 2009. DMSP SSM/I Pathfinder daily EASE-Grid brightness temperatures, Jan 1987–Jul 2008. Boulder, Colorado USA: *National Snow and Ice Data Center Digital media.*

Balsamo, G., C. Albergel, A. Beljaars, S. Boussetta, E. Brun, H. Cloke, D. Dee, E. Dutra, J. Muñoz-Sabater, F. Pappenberger, P. de Rosnay, T. Stockdale, and F. Vitart (2015). ERA-Interim/Land: a global land surface reanalysis data set. *Hydrol. Earth Syst. Sci.,* 19, 389-407, doi: 10.5194/hess-19-389-2015.

Barnett T. P., J. C. Adam, and D.P. Lettenmaier (2005). Potential impacts of a warming climate on water availability in snow-dominated regions. *Nature*, 438, 303-309.

Berezowski, T., Chormaeski, J. and Batelaan, O., 2015. Skill of remote sensing snow products for distributed runoff prediction. Journal of Hydrology, 524, pp.718-732.

Bjørgo E., O. M. Johannessen, and M. W. Miles (1997). Analysis of merged SMMR-SSMI time series of Arctic and Antarctic sea ice parameters 1978 – 1995, *Geophys. Res. Lett*., 24, 413 – 416.

Brown, R., C. Derksen, and L. Wang (2010). A multi-dataset analysis of variability and change in Arctic spring snow cover extent, 1967–2008. *J. Geophys. Res.,* doi:10.1029/2010JD013975.

Brown, R. D. (2010). Analysis of snow cover variability and change in Québec, 1948–2005. *Hydrol. Processe*s, 24, 1929–1954, doi:10.1002/hyp.7565.

Brown, R., and D. Robinson (2011). Northern Hemisphere spring snow cover variability and change over 1922-2010 including an assessment of uncertainty. *The Cryosphere*, 5, 219-229.

Brown, R., and W. P. Mote (2009). The response of Northern Hemisphere snow cover to a changing climate. *J. Climate,* 22, 2124–2145, doi:10.1175/2008JCLI2665.1.

Brown, R., and D. Tapsoba (2007). Improved mapping of snow water equivalent over Quebec. *64th Eastern Snow Conference* St. John's, Newfoundland, Canada.

700 Brown, R. (2007). The Snow Climate of Quebec: A compilation of data sources and information
701 for characterizing the snow cover of Québec. *Ouranos Internal Report* November 27, 2007.
702 Brucker, L., A. Royer, G. Picard, A. Langlois, and M. Fily *(2010),* Hourly simulations of seasonal
703 snow microwave brightness temperature using coupled snow evolution-emission models
704 in Québec, Canada, *Remote Sens. Environ.*, 115, 1966–1977.
705 Chang, A. T. C, J. L. Foster, and D. K. Hall (1996). Effects of forest on the snow parameters
706 derived from microwave measurements during the BOREAS winter field campaign.
707 Hydrol. Processes, 10, 1565-1574.
708 Chang, A. T. C., J. L. Foster, and D. K. Hall (1987). Nimbus-7 derived global snow cover
709 parameters, Ann. of Glaciol., 9, 39-44.
710 Dechant C. and H. Moradkhani (2011). Radiance data assimilation for operational snow and
711 streamflow forecasting. Adv. Water Resou. 34(3), 351–364
712 Derksen C. and A. E. Walker (2003). Identification of Systematic Bias in the Cross-
713 Platform (SMMR and SSM/I) EASE-Grid Brightness Temperature Time Series. IEEE Trans.
714 Geosci. Rem. Sens., 41(4), 910-915.
715 Derksen, C., A. Walker, and B. Goodison (2005). Evaluation of passive microwave snow water
716 equivalent retrievals across the boreal forest/tundra transition of western Canada, Rem.
717 Sens. of Enviro., 96(3–4), 315–327.
718 Derksen, C. (2008). The contribution of AMSR-E 18.7 and 10.7 GHz measurements to improved
719 boreal forest snow water equivalent retrievals. Rem. Sens. of Enviro.. 112: 2700-2709.
720 Derksen, C., and R. Brown (2012). Spring snow cover extent reductions in the 2008-2012 period
721 exceeding climate model projections. Geophys. Res. Lett., 39, doi: 10.1029/2012GL053387.
722 De Sève, D., M. Bernier, J.P. Fortin, and A.E. Walker (1997). Preliminary analysis of the snow
723 microwave radiometry using SSM/I passive microwave data: The case of the La Grande
724 River watershed (Québec). *Ann. of Glaciol.*, 25: 353–361.
725 De Sève D., M. Bernier, J.P. Fortin, and A. Walker (1999). Spatio-temporal analysis of microwave
726 radiometry of snow cover with SSM/I data in a taïga area. *Eastern Snow Conference*.
727 Fredericton, Canada, pp. 200-205, June 1999.
728 De Sève D., N. D. Evora, and D. Tapsoba (2007). Comparison of three algorithms for estimating
729 Snow Water Equivalent (SWE) over the La Grande River watershed using SSM/I data in the
730 context of Hydro- Québec's hydraulic power management. *Conference: Geosci. Rem. Sens.*
731 *Symp., 2007. IGARSS 2007. IEEE International.* DOI: 10.1109/IGARSS.2007.4423791
732 Dong, J., J. P. Walker, and P. R. Houser (2005). Factors Affecting Remotely Sensed Snow Water
733 Equivalent Uncertainty. *Rem. Sens. of Enviro.*, 97(1), 68-82, doi:10.1016/j.rse.2005.04.010.
734 Durand, M., E. J. Kim, and S. A. Margulis (2009). Radiance assimilation shows promise for
735 snowpack characterization, *Geophys. Res. Lett.*, 36, L02503, doi:10.1029/2008GL035214.
736 Foster J. L., C. Sun, J. P. Walker, R. Kelly, A. Chang, J. Dong, and H. Powell (2005). Quantifying
737 the uncertainty in passive microwave snow water equivalent observations. *Rem. Sens. of*
738 *Enviro.,* 94, 187–203
739 Green J., C. Kongoli, A. Prakash, M. Sturm, C. Duguay, and S. Li. (2012). Quantifying the
740 relationships between lake fraction, snow water equivalent and snow depth, and microwave
741 brightness temperatures in an arctic tundra landscape. *Rem. Sens. of Enviro.* 127, 329-340.
742 Hall, D.K., G.A. Riggs, V.V. Salomonson, N.E. DiGirolamo and K.A. Bayr (2002). MODIS snow-
743 cover products, *Rem. Sens. of Enviro.*, 83:181-194.

744 Hallikainen, M., and P. A. Jolma (1992). Comparison of algorithms for retrieval of snow water
745 equivalent from Nimbus-7 SMMR data in Finland. *IEEE Trans. Geosci. Rem. Sens.*, 30(1). 124-
746 131.
747 Hancock S., R. Baxter, J. Evans, and B. Huntley, 2013: Evaluating global snow water equivalent
748 products for testing land surface models. *Rem. Sens. of Enviro.* 128, 107–117.
749 Kang K. K., C. R. Duguay, S. E. L. Howell, C. P. Derksen, and R. E. J. Kelly (2010). Sensitivity of
750 AMSR-E brightness temperatures to the seasonal evolution of lake ice thickness, *IEEE Geosci.*
751 *Rem. Sens. Lett.*, 7(4), 751–755.
752 Kelly, R., A. T. C. Chang, L. Tsang, and J. Foster (2003). A prototype AMSR-E global snow area
753 and snow depth algorithm, *IEEE Trans. Geosci. Rem. Sens.*, *41*(2), 230–242.
754 Kelly, R. E. J. (2009). The AMSR-E Snow Depth Algorithm: Description and Initial Results, *J. of*
755 *The Remote Sensing Society of Japan.* 29(1): 307-317. (GLI/AMSR Special Issue).
756 Klehmet K., Geyer B., Rockel B. (2013). A regional climate model hindcast for Siberia: analysis
757 of snow water equivalent. *The Cryosphere*, 7: 1017-1034.
758 Langlois, A., A. Royer, and K. Goïta (2010). Analysis of simulated and spaceborne passive
759 microwave brightness temperatures using in situ measurements of snow and vegetation
760 properties, *Can. J. Remote Sensing*, 36, S135–S148.
761 Langlois, A., A. Royer, C. Derksen, B. Montpetit, F. Dupont, and K. Goïta (2012). Coupling of
762 the snow thermodynamic model SNOWPACK with the Microwave Emission Model for
763 Layered Snowpacks (MEMLS) for subarctic and arctic Snow Water Equivalent retrievals.
764 *Water Resour. Res.*, 48, W12524, doi:10.1029/2012WR012133.
765 Langlois, A., J. Bergeron, R. Brown, A. Royer, R. Harvey, A. Roy, L. Wang, and N. Thériault,
766 (2014). Evaluation of CLASS 2.7 and 3.5 simulations of snow properties from the Canadian
767 Regional Climate Model (CRCM4) over Québec, Canada. J. of Hydrometeo.
768 doi: http://dx.doi.org/10.1175/JHM-D-13-055.1
769 Lewis, P., GC3mez-Dans, J., Kaminski, T., Settle, J., Quaife, T., Gobron, N., Styles, J. and Berger,
770 M. (2012). An earth observation land data assimilation system (EO-LDAS). Remote Sensing
771 of Environment, 120, pp.219-235.
772 Liu. J. and Z. Li (2013). Temporal series analysis of snow water equivalent of satellite passive
773 microwave data in northern seasonal snow classes (1978-2010). *Proc. of the IEEE International*
774 *Geosci. Rem. Sens. Symposium (IGARSS)*, Melbourne, VIC, 2013, 2013, 3606 – 3609,
775 DOI:10.1109/IGARSS.2013.6723610
776 Luojus, K., J. Pulliainen, M. Takala,C. Derksen,H. Rott,T. Nagler, R. Solberg, A. Wiesmann,S.
777 Metsämäki,E. Malnes, and B. Bojkov (2010). Investigating the feasibility of the GlobSnow
778 snow water equivalent data for climate research purposes. *Geosci. Rem. Sens. Symposium*
779 (IGARSS), 2010 IEEE International (pp. 4851–4853). 25–30 July 2010.
780 doi:10.1109/IGARSS.2010.5741987.
781 Luojus K., J., Pulliainen, M. Takala, J. Lemmetyinen, T. Smolander, and C. Derksen (2014). The
782 GlobSnow Snow Water Equivalent Product. 22 July 2014 – *SnowPEX ISSPI-1*, College Park,
783 Maryland, USA
784 Matzler, C., E. Schanda, and W. Good (1982). Towards the definition of optimum sensor
785 specifications for microwave remote sensing of snow. *IEEE Trans. Geosci. And Rem. Sens.*, GE-
786 20, 57–66.

787 Mätzler, C., 1994: Passive microwave signatures of landscapes in winter. *Meteorol. Atmos. Phys.*,
788 54, 241–260.
789 Meteorological Service of Canada (2000). Canadian Snow Data CD-ROM. CRYSYS Project,
790 Climate Processes and Earth Observation Division, Meteorological Serviceof Canada,
791 Downsview, Ontario.
792 Mote, P. W., 2006: Climate-driven variability and trends in mountain snowpack in western
793 North America. J. Climate, 19, 6209–6220.
794 Mote, P. W., A. F. Hamlet, M. P. Clark, and D. P. Lettenmaier (2005). Declining mountain
795 snowpack in western North America. *Bull. Amer. Meteor. Soc.,* 86, 39–49.
796 Mudryk L. R., C. Derksen, P. J. Kushner and R. Brown (2015). Characterization of Northern
797 Hemisphere snow water equivalent datasets, 1981–2010. *J. of Climate*, DOI: 10.1175/JCLI-D-
798 15-0229.1
799 Ouranos (2015). *Towards Adaptation: Synthesis on climate change knowledge in Québec 2015 Edition*.
800 Summary in English, 13 p. and complete report in French, 415 p., Montréal, Québec, Canada.
801 Available on line http://www.ouranos.ca/en/synthesis2015/
802 Pardé, M., K. Goïta, and A. Royer (2007). Inversion of a passive microwave snow emission
803 model for water equivalent estimation using airborne and satellite data, *Remote Sens.*
804 *Environ.*, 111, 346–356.
805 Pulliainen, J. (2006). Mapping of snow water equivalent and snow depth in boreal and sub-
806 arctic zones by assimilating space-borne microwave radiometer data and ground-based
807 observations. *Rem. Sens. of Enviro.,* 101, 257–269.
808 Pulliainen, J., and M. Hallikainen (2001). Retrieval of regional snow water equivalent from
809 spaceborne passive microwave observations. *Rem. Sens. of Enviro.* 75(1), 76–85.
810 Quaife, T., Lewis, P., De Kauwe, M., Williams, M., Law, B.E., Disney, M. and Bowyer, P. (2008).
811 Assimilating canopy reflectance data into an ecosystem model with an Ensemble Kalman
812 Filter. Remote Sensing of Environment, 112(4), pp.1347-1364.
813 Räisänen, J. (2007). Warmer climate: Less or more snow? Climate Dyn. 30, 307–319,
814 doi:10.1007/s00382-007-0289-y.
815 Rienecker M. M., M. J. Suarez, R. Gelaro, R. Todling, J. Bacmeister, E. Liu, M. G. Bosilovich, S.
816 D. Schubert, L. Takacs, G.-K. Kim, S. Bloom, J. Chen, D. Collins, A.Conaty, A. da Silva, W.
817 Gu, J. Joiner, R. D. Koster, R. Lucchesi, A. Molod, T. Owens, S. Pawson, P. Pegion, C. R.
818 Redder, R. Reichle, F. R. Robertson, A. G. Ruddick, M. Sienkiewicz and J. Woollen (2011).
819 MERRA: NASA's Modern-Era Retrospective Analysis for Research and applications. *J.*
820 *Climate,* 24, 3624–3648. doi: http://dx.doi.org/10.1175/JCLI-D-11-00015.1
821 Rott H., S. H. Yueh D. W. Cline,C. Duguay, R. Essery, C. Haas, F. Hélière, M. G. Kern, E. Malnes,
822 T. Nagler, J. Pulliainen, H. Rebhan , and A. Thompson (2010). Cold Regions Hydrology
823 High-Resolution Observatory for Snow and Cold Land Processes. *IEEE Proceedings*, 98 (5):
824 752-765. doi: http://dx.doi.org/10.1109/JPROC.2009.2038947.
825 Roy, V., K. Goïta,A. Royer, A. Walker, and B. Goodison (2004). Snow water equivalent retrieval
826 in a Canadian boreal environment from microwave measurements using the HUT snow
827 emission model. *IEEE Trans. Geosci. Rem. Sens.*, 42(9), 1850–1859.
828 Roy A., A. Royer, B. Montpetit, and A. Langlois (2015). Microwave snow emission modeling of
829 boreal forest, *Proc. of the Int. Geosci. Rem. Sens. Symp. 2015* (IGARSS 2015) Paper #8044, July
830 26-31, 2015, Milan, Italy, 4 p.

831 Roy, A., Royer, A., Wigneron, J.-P., A. Langlois, J. Bergeron and P. cliché (2012). A simple
832 parameterization for a boreal forest radiative transfer model at microwave frequencies. *Rem.*
833 *Sens. of Enviro.* 124, 371–383.
834 Roy, A., A. Royer, R. Turcotte (2010). Improvement of springtime streamflow simulations in a
835 boreal environment by incorporating snow-covered area derived from remote sensing data.
836 *J. Hydrology*, 390, 35–44
837 Royer A., and S. Poirier (2010). Surface temperature spatial and temporal variations in North
838 America from homogenized satellite SMMR-SSM/I microwave measurements and
839 reanalysis for 1979–2008. *J. Geophys. Res. Atmospheres*, 115 D08110.
840 Schultz, G. A., and E. C. Barrett (1989). Advances in remote sensing for hydrology and water
841 resources management. *Tech. Doc. In Hydrology, UNESCO,* 102 pp.
842 Seidel K. and J. Martinec (2004). Remote Sensing in Snow Hydrology: Runoff Modelling, Effect
843 of Climate Change. *Springer-Verlag Berlin Heidelberg New-York, 150p.*
844 SeNorge (2009). Normal annual maximum of snow amount in mm for normal period 1961-1990.
845 *Norwegian Water Resources and Energy Directorate and the Norwegian Meteorological Institute*.
846 Available at: http://senorge.no
847 Sospedra-Alfonso, R., Mudryk, L., Merryfield, W. and Derksen, C., 2016. Representation of
848 Snow in the Canadian Seasonal to Interannual Prediction System. Part I: Initialization.
849 Journal of Hydrometeorology, 17(5), pp.1467-1488.
850 Stewart, I. T., D. R. Cayan, and M. D. Dettinger (2005). Changes toward earlier streamflow
851 timing in western North America, *J. Clim*ate, 18, 1136 – 1155.
852 Sturm, M., H. Olmgren and G. E. Liston (1995). A seasonal snow cover classification scheme
853 for local to global applications. *J Climate*, 8 (5), Part 2, 1261- 1283.
854 Sturm, M., and G.E. Liston (2003). The snow cover on lakes of the arctic coastal plain of Alaska,
855 USA. *J. Glaciology*, 49, 370–380.
856 SWIPA (2011). *Snow, Water, Ice, and Permafrost in the Arctic (SWIPA)*, Executive Summary, Arctic
857 Monitoring and Assessment Program (AMAP) Secretariat. Oslo, Norway, available at: www.
858 amap.no, 16 pp., 2011.
859 Takala, O. M., J. Pulliainen,S. Metsämäki, and J. Koskinen (2009). Detection of snowmelt using
860 spaceborne microwave radiometer data in Eurasia From 1979 to 2007. *IEEE Trans. Geosci.*
861 *Rem. Sens.*, 47, 2996–3007.
862 Takala, M., K. Luojus, J. Pulliainen, C. Derksen, J. Lemmetyinen, J.-P. Kärnä, J. Koskinen, and
863 B. Bojkov (2011). Estimating northern hemisphere snow water equivalent for climate
864 research through assimilation of space-borne radiometer data and ground-based
865 measurements, *Rem. Sens. of Enviro.*, 115(12), 3517–3529.
866 Tapsoba, D., V. Fortin, F. Anctil, and M. Haché (2005). Apport de la technique du krigeage avec
867 dérive externe pour une cartographie raisonnée de l'équivalent en eau de la neige :
868 Application aux bassins de la rivière Gatineau. *Can. J. Civil Engineering,* 32(1), 289-297(9).
869 Tedesco, M., R. Kelly, J. L. Foster, and A. T. C. Chang. (2004). *AMSR-E/Aqua Daily L3 Global*
870 *Snow Water Equivalent EASE-Grids. Version 2. Boulder, Colorado USA: NASA National Snow and*
871 *Ice data center Distributed Active Archive Center.* doi: 10.5067/AMSR-E/AE_DYSNO.002.
872 Tong, J., S. Dery,P. Jackson, and C. Derksen (2010). Testing snow water equivalent retrieval
873 algorithms for passive microwave remote sensing in an alpine watershed of western Canada.
874 *Can. J. Rem. Sens.*, 36(S1), 74–86.

875 Touré A., K. Goïta, A. Royer, E. Kim, M. Durand, S. A. Margulis and H. Lu (2011). A Case Study
876 of Using a Multi-Layered Thermo-Dynamical Snow Model for Radiance Assimilation. *IEEE*
877 *Trans. Geosci. Rem. Sens.*, 49(8), 2828-2837.
878 Turcotte R., L.-G. Fortin, V. Fortin, J.-P. Fortin, and J.- P. Villeneuve (2007). Operational analysis
879 of the spatial distribution and the — temporal evolution of the snowpack water equivalent
880 in ǀsouthern Quebec, Canada, *Hydrology Research*, 38 (3) 211-234; DOI: 10.2166/nh.2007.009
881 Turcotte R., Fortier-Filion, T.-C., Fortin, V., Roy, A., and Royer, A. (2010). Simulation
882 hydrologiques des derniers jours de la crue du printemps : le problème de la neige
883 manquante. *Hydrological Sciences Journal*, 55(6): 872-882, DOI: 10.1080/02626667.2010.503933
884 Urban M., M. Forkel, J. Eberle, C. Hüttich, C. Schmullius and M. Herold (2014). Pan-Arctic
885 Climate and Land Cover Trends Derived from Multi-Variate and Multi-Scale Analyses
886 (1981–2012). *Remote Sens.*, 6, 2296-2316; doi:10.3390/rs6032296
887 Vachon, F., K. Goïta, D. De Sève, and A. Royer (2010). Inversion of a Snow Emission Model
888 calibrated with in situ data for snow water equivalent monitoring. *IEEE Trans. Geosci. Rem.*
889 *Sens.*, 48(1), 59–71.
890 Vachon F., D. De Sève, Y. Choquette and F. Guay (2012). SWE retrieval over a forested
891 watershed using a snow emission model inversion algorithm. *Proc. of the 2012 IEEE*
892 *International Geosci. Rem. Sens. Symp.*, Munich, Ge, 4414-4417. doi:
893 10.1109/IGARSS.2012.6350394
894 Vachon, F., D. De Sève, Y. Choquette and F. Guay (2015). SWE monitoring during the winter
895 and spring melt by combining microwaves remote sensing data, modeling and ground
896 data. *Proc. of the IEEE International Geosci. Rem. Sens. Symp. (IGARSS-2015)*, 5201 – 5204.
897 Vikhamar-Schuler, D. S. Beldring, E.J. Førland, L.A. Roald and T. Engen-Skaugen (2006). *Snow*
898 *cover and snow water equivalent in Norway: current conditions (1961-1990) and scenarios for the*
899 *future (2071-2100)*. met.no climate report no. 01/2006, Norwegian Meteorological Institute,
900 Oslo, Norway.
901 Vincent, L. A., X. Zhang, R. Brown, Y. Feng, E.J. Mekis, E. Milewska, H. Wan, and X.L. Wang
902 (2015). Observed trends in Canada's climate and influence of low-frequency variability
903 modes, *J. Climate,* 28, 4545–4560. WMO (1994) Guide to Hydrological Practices, 5th edn, vol.
904 1. WMO-No. 168. World Meteorological Organization, Geneva, Switzerland.
905 Yang, J., Y. Ding, S. Liu, and J. -F. Liu (2007). Variations of snow cover in the source regions of
906 the Yangtse and Yellow Rivers in China between 1960 and 1999. *J. Glaciol.*, 53, 420–426.
907 Zhang, X, R Brown, L Vincent, W Skinner, Y Feng and E Mekis. (2011). Canadian climate trends,
908 1950-2007. Canadian Biodiversity: Ecosystem Status and Trends 2010, Technical Thematic
909 Report No. 5. Canadian Councils of Resource Ministers. Ottawa, ON.
910

911 **List of Figure captions**

912 **Fig. 1.** (a) Location map of the study region (Eastern Canada); (b) Land Cover Map
913 (LCM, 2005) classification for Eastern Canada aggregated into eight classes and on
914 the 25x25-km EASE-Grid projection.

915 **Fig. 2**. Location of snow courses in the *in situ* SWE database (1980 to 2009). The blue
916 stars are the superposition of the Hydro-Québec (yellow stars) and MSC/MDDEP
917 snow surveys (blue points), sometimes taken at the same station over the 30-years
918 period.

919 **Fig. 3**. Mean distance (in kilometers) between SD observations used by GS-2 project and
920 EASE-Grid cells on which the GS-2 SWE are projected. The SD observations are
921 those used by GS-2 from 1980 to 2012 (R. Brown, personal communication, 2016).

922 **Fig. 4.** GS-2 SWE product estimates as a function of *in situ* SWE measurements. The
923 black vertical dotted line represents the saturation limit defined for this study. The
924 Y=X line is also plotted in black.

925 **Fig. 5.** Corresponding seasonal snow classification, based on Sturm et al. (1995), of the
926 ground-based SWE measurements with the database without SWE_{gb}>150 mm.
927 **Erreur ! Signet non défini.**

928 **Fig. 6.** Analysis for the dataset with SWE_{gb}<150mm and over the October to May period
929 (1980-2009): (a) Monthly biases (SWE_{GS} - SWE_{gb}) according to the Sturm et al. (1995)
930 seasonal snow classification; (b) Number of data points (SWE_{gb}) for each month by
931 snow category: tundra (red), taiga (green), maritime snow (blue) and mountain
932 snow (yellow).

933 **Fig. 7.** Global performance statistics for each processing step: the entire dataset with
934 matching data (black, Step 1), only with SWE_{gb}<150mm (blue, Step 2) and over the
935 January-February time period (red, Step 3). The graphs present the inter-annual
936 variability of the unbiased RMSE (a); the inter-annual variability of the bias (b) and

the inter-annual variability of the average SWE_{GS} (c). The dotted lines are the average of the time series from 1980 to 2009.

Fig. 8. Unbiased RMS according to the forest cover fraction (in %). The unbiased RMS is fitted with a simple quadratic function (black dotted line).

Fig. 9. Evaluation of the GS-2 database for Eastern Canada, SWE_{GS} are compared to ground-based measurements (using Database 3) for each land cover class: (a) Coniferous; (b) Deciduous; (c) Mixed forest; (d) Herbaceous; (e) Tundra. The color scale represents the data density of scattered points, computed by using circles (radius of 20) centered at each data point.

Fig. 10. The $SWE_{AMSR\text{-}E}$ and GS-2 SWE results are compared to *in situ* observations from 2002 to 2009, for January-February only.

Fig. 11. (a) Annual mean SWE anomaly time series, associated with the standard deviations for both datasets (ground database in red and GS-2 database in black), and over the southern area, defined by the herbaceous and deciduous areas**.** (b) Same as (a) for the northern area, defined by the coniferous and tundra areas. (c) Same as (a) for the maximum SWE anomaly time series. (d) Same as (b) for the maximum SWE anomaly time series. The lines represent the linear SWE regression in time. The complete Hydro-Québec database from 1980 to 2009 was used, over a December to March period.

Fig. 12. Anomaly trend in the annual SWE_{max} for the 1980-2009 period using the GS-2 time series.